Opto-Electronic Advances

CN 51–1781/TN ISSN 2096–4579 (Print) ISSN 2097–3993 (Online)

Sequential harmonic spin–orbit angular momentum generation in nonlinear optical crystals

Yutao Tang, Zixian Hu, Junhong Deng, Kingfai Li and Guixin Li

Citation: Tang YT, Hu ZX, Deng JH, et al. Sequential harmonic spin–orbit angular momentum generation in nonlinear optical crystals. *Opto-Electron Adv* **7**, 240138(2024).

https://doi.org/10.29026/oea.2024.240138

Received: 6 June 2024; Accepted: 13 September 2024; Published online: 16 December 2024

Opto-Electronic Advances

Article

December 2024, Vol. 7, No. 12

DOI: 10.29026/oea.2024.240138 CSTR: 32247.14.oea.2024.240138

Sequential harmonic spin–orbit angular momentum generation in nonlinear optical crystals

Yutao Tang[1†], Zixian Hu[1†], Junhong Deng[1], Kingfai Li[1] and Guixin Li[1,2*]

Light beams carrying multiple orbital angular momentum (OAM) states, which can be realized by the structured media with phase singularities, have attracted great attentions in the fields of high dimensional optical information processing. Alternatively, a simple uniaxial crystal can be used to simultaneously generate four OAM states of light through the second harmonic generation and cascaded optical spin–orbit interaction (SOI) processes. However, two of the OAM states realized in the crystal are very weak and limit the practical applications. Here, we aim to circumvent this constraint by using the sequential optical SOI processes in two crystals with threefold rotational symmetry. Four angular momentum states of the fundamental waves are prepared after the first crystal and then are utilized to generate the corresponding second harmonic waves (SHWs) with opposite spin and doubled OAM in the second crystal. Further through a sequential SOI process, totally eight angular momentum states of the SHWs with nearly equal energy are experimentally observed. The proposed methodology may find potential applications in optical communications, parallel optical computing, optical manipulation and so on.

Keywords: angular momentum of light; nonlinear optics; second harmonic generation; optical spin–orbit interaction

Tang YT, Hu ZX, Deng JH et al. Sequential harmonic spin–orbit angular momentum generation in nonlinear optical crystals. *Opto-Electron Adv* **7**, 240138 (2024).

Introduction

Orbital angular momentum (OAM) of photons, manifested by the phase singularities[1] and unlimited number of mutually orthogonal states, has been proved to hold great potentials in optical imaging[2,3], optical manipulations[4–6], optical communications[7,8], information multiplexing[9], and quantum information processing[10–12], etc. Methods on generating OAM-carrying vortex beams and relevant applications have been developed from traditional spiral phase plates[13,14] and liquid crystal based diffractive optical elements[15] to spatial light modulators[16,17], optical metasurfaces[18–21], photonic crystals[22], and on-chip vortex lasers[23,24]. Recent studies show that optical spin–orbit interaction (SOI)[25,26] represents a novel way for OAM generations by utilizing the mutual conversions between the spin angular momentum (SAM) and OAM of photons, via structured media[15,27] or anisotropic optical crystals[28,29].

In the meantime, nonlinear optical processes in materials will definitely introduce new degrees of freedom for manipulating the light fields and have been attracting scientists' attention. Moreover, OAM-related structured

[1]Department of Materials Science and Engineering, Southern University of Science and Technology, Shenzhen 518055, China; [2]Institute for Applied Optics and Precision Engineering, Southern University of Science and Technology, Shenzhen 518055, China.

[†]These authors contributed equally to this work.

*Correspondence: GX Li, E-mail: ligx@sustech.edu.cn

Received: 6 June 2024; Accepted: 13 September 2024; Published online: 16 December 2024

light[30] in nonlinear optical regime has also been widely explored[31], such as generation of spatiotemporal OAM light in SHG process[32] and toroidal light pulses[33]. Early works studying the conservation law of OAM in the second harmonic generation (SHG) process[34] are reported soon after the proposal of OAM of light. In recent years, nonlinear photonic metasurfaces[35–37] and photonic crystals[38,39] provide new platforms for generating the OAM states of photons at the second and third harmonic frequencies. By virtue of the unlimited OAM modes of photons, a myriad of classical or quantum applications have entered into the high-dimensional realm[40–42]. In addition, the spatiotemporal properties of the optical vortices are experimentally demonstrated in both linear and nonlinear optical regimes[30,32,43].

One interesting topic in the OAM community is to simultaneously generate the high dimensional OAM states of light. In linear optics, many kinds of artificial media, such as diffractive optical elements[10] and optical metasurfaces[12,44], have been successfully utilized to realize this target. It should be noticed that a uniaxial optical crystal can be also used to produce two kinds of OAM states of light through the SOI process. The SOI conversion efficiency is up to 50% and no alignment to the singularity point is needed[29] as that in the conventional diffractive optical element. Previously, we show how to generate four angular momentum states in the SHG process, in which the β-BBO crystal is pumped by the circularly polarized fundamental wave (FW)[45]. In such a strategy, two angular momentum states of the FWs coming from the linear SOI process are used to generate the corresponding angular momentum states of the SHWs. Then, the SHWs experience a cascaded SOI process, leading to four angular momentum states in total. Since the complex light–matter interactions occur in a single crystal, the conversion efficiencies of two angular momentum modes of the SHWs are much stronger than the other two, making it difficult to use all the angular momentum states.

To circumvent this constraint, here we propose the concept of sequential optical spin–orbit interactions to achieve eight angular momentum states of the SHWs with nearly equal conversion efficiency. As shown in Fig. 1, the experimental configuration consists of two sequential β-BBO crystals with threefold (C_3) rotational symmetry. In the first crystal, the linear SOI process leads to two angular momentum states of the FWs with almost the same energy. By flipping the SAM states of the FWs with polarization optics before the second crystal, we are able to obtain two new angular momentum states of the FWs. After being refocused into and passing through the second BBO crystal, the four FW states generate four angular momentum states of the SHWs (see Supplementary information Section 1). Further through a sequential linear SOI process, the SHWs carry eight angular momentum states with almost the same energy.

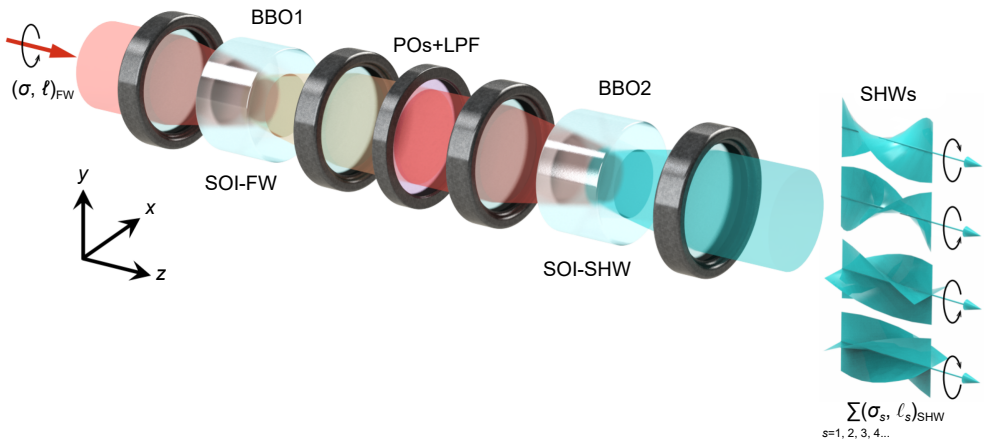

Fig. 1 | Generation of second harmonic waves (SHWs) with multiple angular momentum states through sequential optical spin–orbit interactions (SOIs) in two BBO crystals with threefold rotational symmetry. For a circularly polarized fundamental wave (FW) with angular momentum state of $(\sigma, \ell)_{FW}$, two states of the FWs will be generated in BBO1 through optical SOI process. Then the spin angular momentum state of the two states can be flipped by using an assembly of polarization optics (POs) after BBO1. Therefore, totally four kinds of angular momentum states of the FWs are prepared after the first crystal. The SHWs generated in BBO1 are blocked by using the long-pass filter (LPF). Then, by refocusing the FWs into the second BBO crystal, the SHWs with four corresponding angular momentum states are generated in the Direct channels. Through a sequential SOI process of the SHWs in the second BBO crystal, four new angular momentum states are obtained. It is expected that these eight kinds of angular momentum states of SHWs have nearly equal energies.

Results and discussion

Spin–orbit interaction of the SHWs in one BBO crystal

Firstly, the generation and spin–orbit interaction process of the SHWs in one BBO crystal is revisited[46]. From the symmetry selection rules in nonlinear optics[47–50], when a circularly polarized FW propagates along the rotational axis of a crystal possessing m-fold rotational symmetry, the allowed orders of harmonic generation are $n = pm \pm 1$, p is an integer, and the '+' or '–' sign means that the circular polarization state of the harmonic wave is same as or opposite to that of the FW. In this work, the FW is propagating along the C_3 rotational axis of the BBO crystal ($m = 3$), therefore the SHW ($n = 2$) with opposite circular polarization to that of the FW can be generated. In this process, two FW photons with SAM of $\sigma\hbar$ are annihilated to create a second harmonic photon with SAM of $-\sigma\hbar$, where $\sigma = \pm 1$ represents the left or right circular polarization states (LCP/RCP) of the FW, and $\hbar$ is the reduced Plank's constant. The SAM difference of $-3\sigma\hbar$ before and after the SHG process is offset by the BBO crystal. In the meantime, if the FW carry an OAM of $\ell\hbar$ per photon, the SHW photon should carry an OAM of $2\ell\hbar$ as a result of the conservation law of OAM[34]. To sum up, if we denote the SAM and OAM states of photons by (σ, ℓ), the SHG process in the BBO crystal can be represented as $(\sigma, \ell)_{\rm FW} + (\sigma, \ell)_{\rm FW} \rightarrow (-\sigma, 2\ell)_{\rm SHG}$.

When the FW is focused into the BBO crystal with C_3 rotational symmetry, both the FW and the SHW experience the SOI processes, where the SAM of light is flipped and its difference is imparted into the OAM of light. Such a process can be briefly represented as $(\sigma, \ell) \rightarrow (-\sigma, \ell + 2\sigma)$, from which one can easily see the conservation of the total angular momentum of light. Due to the SOI effect, the angular momentum state $(\sigma, \ell)_{\rm FW}$ of the input FW will be converted to two states, $(\sigma, \ell)_{\rm FW}$ and $(-\sigma, \ell + 2\sigma)_{\rm FW}$, which then generate the SHWs with angular momentum states of $(-\sigma, 2\ell)_{\rm SHG}$ and $(\sigma, 2\ell + 4\sigma)_{\rm SHG}$ in the BBO crystal. The generated SHWs in the same BBO crystal also experience a SOI process, forming four angular momentum states, namely $(-\sigma, 2\ell)_{\rm SHG}$, $(\sigma, 2\ell - 2\sigma)_{\rm SHG}$, $(\sigma, 2\ell + 4\sigma)_{\rm SHG}$, and $(-\sigma, 2\ell + 6\sigma)_{\rm SHG}$. For convenience, we denote these four angular momentum states as s_1 to s_4 in the following discussions. However, the last two angular momentum states s_3 and s_4 of the SHWs, which are expressed as $(\sigma, 2\ell + 4\sigma)_{\rm SHG}$ and $(-\sigma, 2\ell + 6\sigma)_{\rm SHG}$ respectively, have quite low efficiency.

Figure 2 shows the results of the single crystal case, in which the SHW from the SOI-induced FW is very weak[45]. As shown in Fig. 2(a), we mainly consider the SHWs with angular momentum states of $(-\sigma, 2\ell)_{\rm SHG}$, $(\sigma, 2\ell - 2\sigma)_{\rm SHG}$. Then, we carry out the nonlinear optical

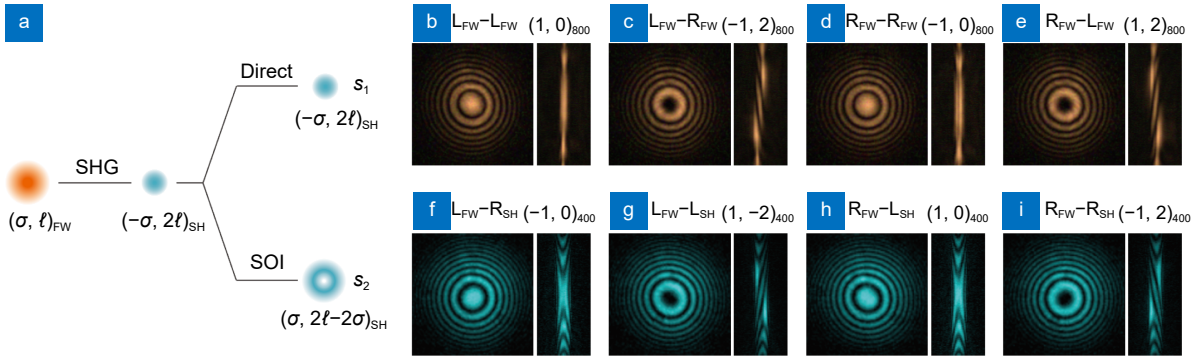

Fig. 2 | The linear and nonlinear optical spin–orbit interactions (SOIs) in one BBO crystal. (**a**) Schematic diagram of the linear and nonlinear optical SOI processes in one BBO crystal. The BBO crystal with threefold rotational symmetry is placed at the center of a pair of 10× objective lenses to enhance the SOI effect. For a fundamental wave (FW) with angular momentum state of $(\sigma, \ell)_{\rm FW}$, the two output states of the SHWs come from the Direct and SOI channels are $(-\sigma, 2\ell)_{\rm SH}$ and $(\sigma, 2\ell - 2\sigma)_{\rm SH}$, respectively. (**b**–**e**) Circular polarization resolved intensity profiles of the FWs (λ = 800 nm) after the BBO crystal. The incident FW is left- or right- circularly polarized (L/R) and the images for the L/R components of the output FWs are experimentally recorded. For each circular polarization combination, two images of the FWs are recorded by using a spherical lens (left panel) and a cylindrical lens (right panel). The dark core of the intensity profile imaged through the spherical lens is the typical characteristic of a vortex beam, and the value of the topological charge is revealed by the dark fringes in the one imaged via the cylindrical lens. (**f**–**i**) Circular polarization resolved intensity profiles of the second harmonic waves (λ = 400 nm) generated in the BBO crystal are also recorded. It should be noted that the SHWs measured here mainly come from the Direct FW channel, as that of the SOI-induced FW channel are very weak. The color of the SHW images is converted from the original blue to cyan for better visualization of the intensity patterns.

experiments to verify our assumption. In the experiment, a femtosecond laser (pulse duration: ~140 fs, repetition frequency: 80 MHz) is used to pump the BBO crystal (see Methods and Supplementary information Section 2). The crystal is coated with 400 nm/800 nm anti-reflection layers on its two facets, therefore the preferred fundamental wavelength is set to be 800 nm. We focus on the case of a circularly polarized Gaussian FW with angular momentum state of $(\pm1, 0)_{\mathrm{FW}}$. The FW is focused into the BBO crystal by using an objective lens with numerical aperture of $NA = 0.25$. Both the FW and the SHW behind the crystal are collected by the second objective lens with the same NA. When the input FW state is $(1, 0)_{\mathrm{FW}}$, the measured intensity profiles of the output FWs with LCP and RCP states are shown in Fig. 2(b, c), which are captured by using a spherical lens (left panel) and a cylindrical lens (right panel), respectively. While through the spherical lens images we are able to observe the doughnut shaped intensity profile of the vortex beam, the cylindrical lens images can be used to distinguish the sign and value of the OAM states of light[51]. From Fig. 2(b, c), we can see that the two angular momentum states $(1, 0)_{\mathrm{FW}}$ and $(-1, 2)_{\mathrm{FW}}$ of the output FW have comparable intensities. Similar results corresponding to input FW with angular momentum state $(-1, 0)_{\mathrm{FW}}$ are shown in Fig. 2(d, e), in which the output angular momentum states are $(-1, 0)_{\mathrm{FW}}$ and $(1, -2)_{\mathrm{FW}}$, respectively.

As shown in Fig. 2(f–i), the intensity profiles of the SHWs are obtained by filtering out the FW after the BBO crystal. For the FW with angular momentum state of $(1, 0)_{\mathrm{FW}}$, two SHW states of $(-1, 0)_{\mathrm{SHG}}$ and $(1, -2)_{\mathrm{SHG}}$ can be well observed (Fig. 2(f, g)), corresponding to states s_1 and s_2 in the SHG process. While s_1 is the direct harmonic generation from the input FW, s_2 is the linear SOI-induced state from s_1. The states s_3 and s_4 generated from the SOI-induced FW of $(-1, 2)_{\mathrm{FW}}$, are very weak and difficult to be measured. When the angular momentum state of the FW is switched to $(-1, 0)_{\mathrm{FW}}$, similar phenomena can be found in Fig. 2(h, i). These results are consistent with the previous ones discussed in ref.[45]. It should be noted that the SHW at state s_2 has almost the same energy as that of s_1 (see Supplementary information Section 3).

Sequential optical SOI processes with two BBO crystals

Based on the above analysis, we propose to achieve the uniform energy distributions of the angular momentum states of the SHWs by using the sequential optical SOI processes in two BBO crystals. The first crystal and an assembly of polarization optics are utilized to prepare the four FW states with a near 50% SOI conversion efficiency, and the second crystal provides the channel for generating the SHWs as well as the SOI process. Figure 3(a) shows the experimental setup used to generate the eight SHW states with the sequential SOI processes. For a circularly polarized FW with Gaussian beam profile, the LCP and RCP components of the FWs with specific orbital angular momentum states are first prepared with BBO1, and then refocused into BBO2. To avoid the complex interferences of the SHWs generated from the two crystals, the SHWs generated from BBO1 are filtered out by using a long-pass filter.

The angular momentum states of the FWs after BBO2 are recorded and shown in Fig. 3(b–q) (see Supplementary information Section 4). For each circularly polarized FW state leaving from BBO1, as shown in Fig. 2(b–e), it experiences the linear SOI process and is partially converted to the one with opposite circular polarization. The circular polarization states of the FWs at the input, after BBO1, before and after BBO2 are labelled in Fig. 3(b–q). For the case of input FW state $(1, 0)_{\mathrm{FW}}$, the one focused into BBO2 is $(1, 0)_{\mathrm{FW}}$ when the '$\mathrm{L_{FW}}$-$\mathrm{L_{FW}}$' polarization combination is chosen after BBO1 (Fig. 3(b, c)). The FW continues to experience a linear SOI process in BBO2, leading to two FW states, namely $(1, 0)_{\mathrm{FW}}$ in Fig. 3(b) and $(-1, 2)_{\mathrm{FW}}$ in Fig. 3(c). When the circular analyzer (QWP2 and LP2) after BBO1 is switched to the RCP condition ('$\mathrm{L_{FW}}$-$\mathrm{R_{FW}}$'), we can extract the SOI-induced FW state, which is $(-1, 2)_{\mathrm{FW}}$. This state remains unchanged in BBO2, as shown in Fig. 3(d), or is converted back to an OAM-free state of $(1, 0)_{\mathrm{FW}}$ through one more linear SOI process (Fig. 3(e)). It should be noted that although the spherical lens image in Fig. 3(e) exhibits a ring-like pattern, the cylindrical lens image clearly shows that the FW carries no OAM. In addition, the experimental setup in Fig. 3(a) offers a convenient way to control the SAM state of the FWs after BBO1 by controlling the fast axis direction of QWP3. If the fast axis of QWP3 is rotated by an angle of 90°, the SAM state of the FW before BBO2 can be flipped from LCP to RCP ('$\mathrm{L_{FW}}$-$\mathrm{L_{FW}}$-$\mathrm{R_{FW}}$' as in Fig. 3(j–k)), or from RCP to LCP ('$\mathrm{L_{FW}}$-$\mathrm{R_{FW}}$-$\mathrm{L_{FW}}$' as in Fig. 3(l–m)), therefore leading to four new angular momentum states of the FWs after BBO2, thanks to the SOI process of the FWs in BBO2. Similar

results can also be observed with the input FW state of $(-1, 0)_{\mathrm{FW}}$, as shown in Fig. 3(f–i) and Fig. 3(n–q).

Figure 4 shows the angular momentum states of the SHWs observed after BBO2 for FW states of $(1, 0)_{\mathrm{FW}}$ and $(-1, 0)_{\mathrm{FW}}$. From the knowledge learnt in Fig. 2, we will focus on the efficient generation of SHWs from the Direct FW channel. In the case of $(1, 0)_{\mathrm{FW}}$, the four angular momentum states (Fig. 3(b, d, j, l)) of the Direct FWs prepared with BBO1 have almost the same energy. The corresponding four Direct-generated SHW states (Fig.

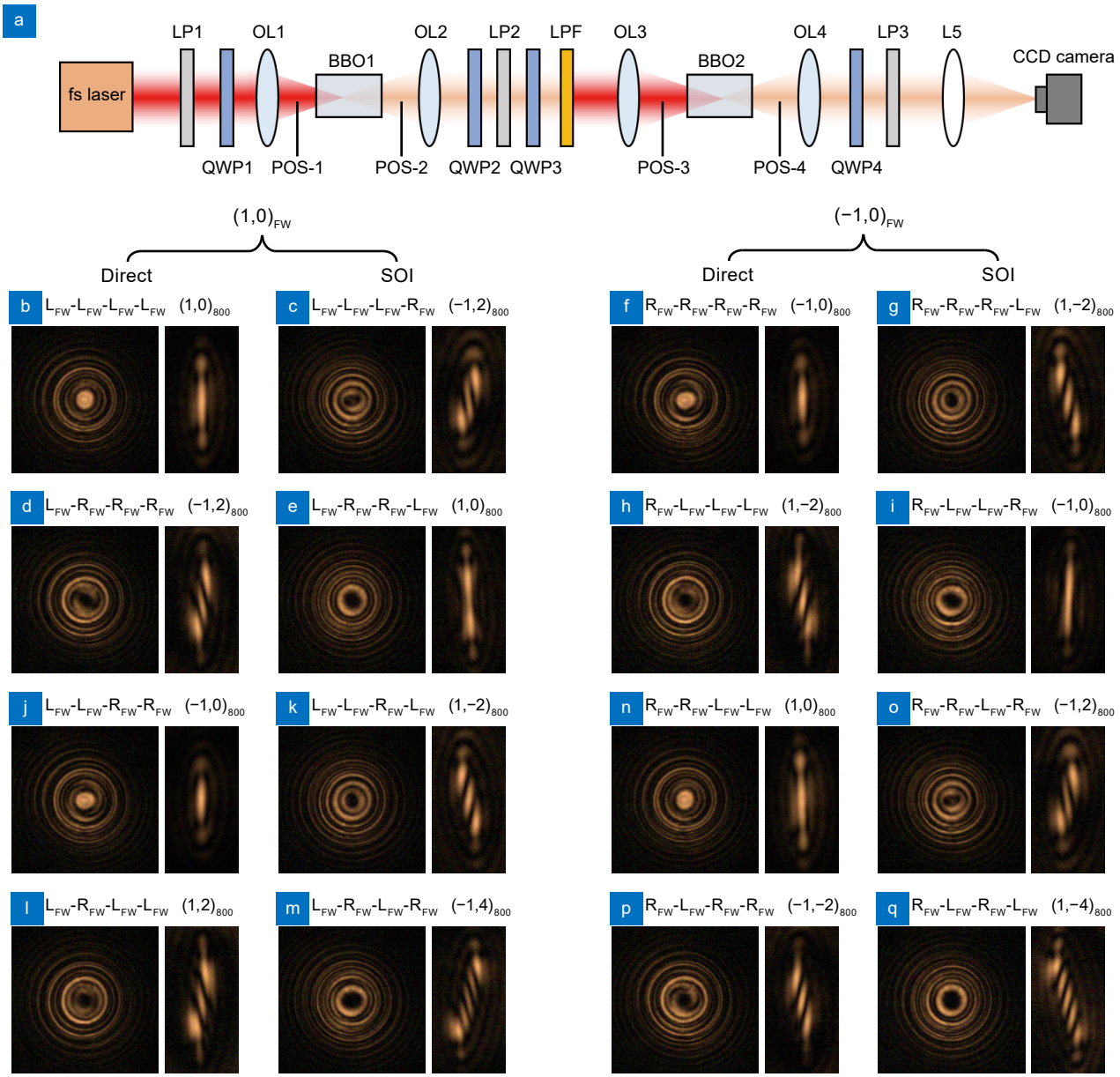

Fig. 3 | The sequential optical spin–orbit interaction process of the fundamental waves (FWs) in the double BBO crystal system. (**a**) Schematic illustration of the double BBO crystal system which consists of two confocal optical sections. Each section includes a pair of 10× OLs (objective lenses) and a BBO crystal. LP (linear polarizer) and QWP (quarter-wave plate) are used to generate or analyze the circularly polarized FWs and second harmonic waves (SHWs). The combination of QWP2, LP2 and QWP3 is used to prepare the specific circular polarization component of the outgoing FWs from the first crystal (BBO1). LPF, long-pass filter, which is used to block the SHWs generated in BBO1. QWP4 and LP3 are used to analyze the circular polarization states of the SHWs generated in the second crystal (BBO2). L5, tube lens (spherical or cylindrical lens). (**b–q**) Intensity profiles of the FWs behind BBO2. The polarization labels above the results correspond to the sixteen combinations of the circular polarization states (L/R) of the FWs at the positions marked as POS-1 to POS-4 in (a). Compared to the results in (b) to (i), the ones in (j) to (q) are obtained under the conditions that the spin angular momentum states of the FWs between POS-2 and POS-3 are flipped from LCP to RCP, or from RCP to LCP by rotating the fast axis direction of QWP3.

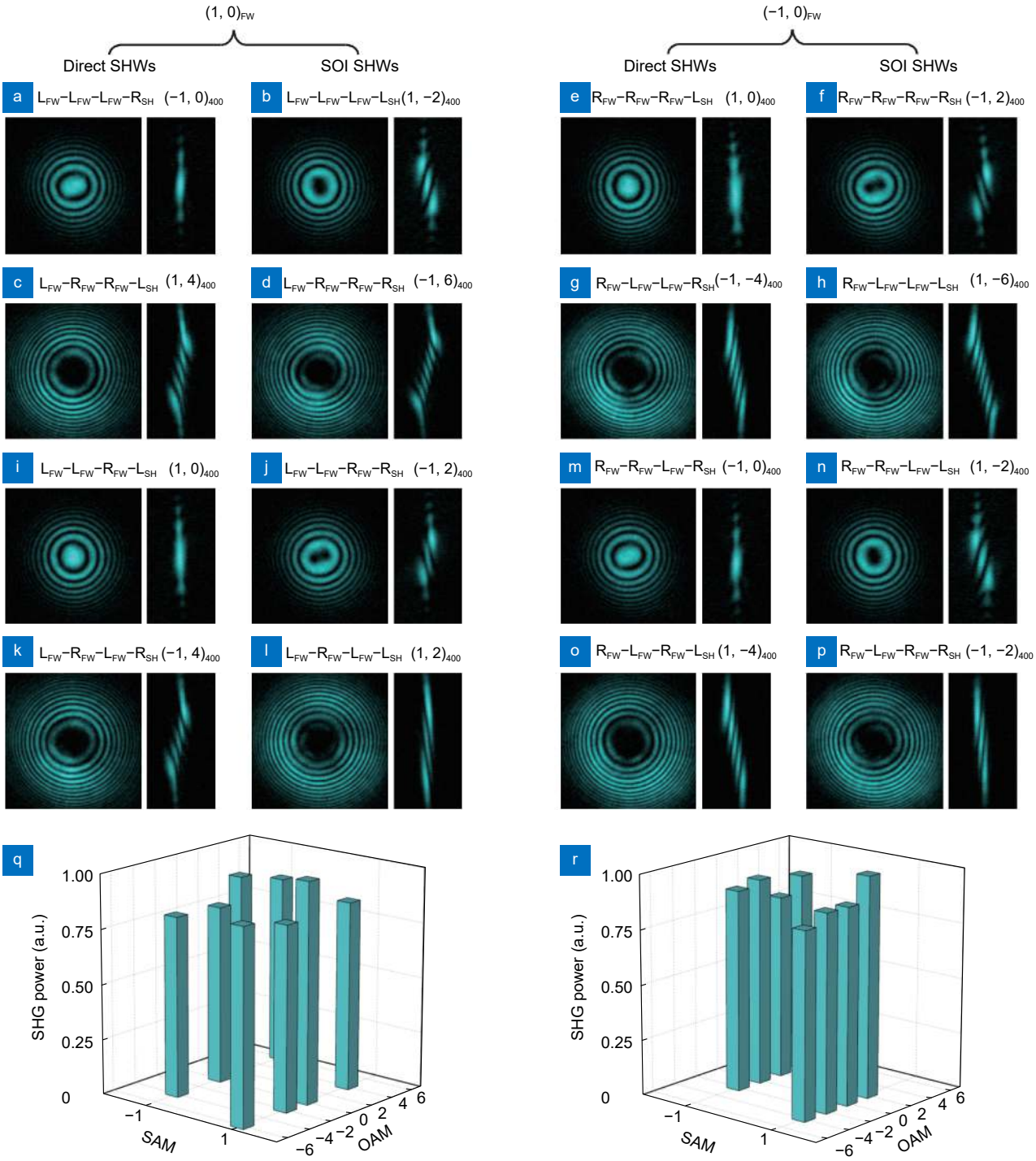

Fig. 4 | Angular momentum states of the second harmonic waves (SHWs) through the sequential spin–orbit interactions (SOIs) in the double BBO crystal system. The experimental setup is the same as the one shown in Fig. 3(a). (**a**–**p**) Sixteen cases correspond to full combinations of the circular polarization states of the fundamental waves (FWs) that are incident on and after BBO1, before BBO2 and that of the SHWs after BBO2 (corresponding positions are marked as POS-1 to POS-4 in Fig. 3(a)). When the angular momentum state of the input FW is LCP and Gaussian, i.e. $(1, 0)_{FW}$, the double crystal system can generate eight angular momentum states of the SHWs, as revealed in (a) to (d) and (i) to (l). The energies of the eight states are nearly the same as each other. While in (a) to (h) the spin angular momentum states of the FWs are kept unchanged, they are flipped from LCP to RCP, or from RCP to LCP in (i) to (p), which is realized by rotating the fast axis direction of QWP3. (**q**, **r**) The normalized relative power distributions of the angular momentum states of SHWs, where (q) and (r) correspond to the cases for input FW states of $(1, 0)_{FW}$ and $(-1, 0)_{FW}$, respectively. SAM, spin angular momentum; OAM, orbital angular momentum.

4(a, c, i, k)) in BBO2 have similar nonlinear conversion efficiencies. In the meantime, another four angular momentum states (Fig. 4(b, d, j, l)) of the SHWs are generated through the linear SOI process of the SHWs in BBO2. From the spherical and cylindrical lens images shown in Fig. 4(a–d), one can easily distinguish the angular momentum states of the SHWs, which are $(-1, 0)_{\rm SHG}$, $(1, -2)_{\rm SHG}$, $(1, 4)_{\rm SHG}$ and $(-1, 6)_{\rm SHG}$, corresponding to the s_1 to s_4 states discussed in previous section. It should be noted that all the generated angular momentum states here originate from the Direct FWs. More importantly, the intensities of these four states are almost equally distributed, with a standard deviation of ~1.2% as evaluated from the SHW spectra recorded by using a spectrometer (see Supplementary information Section 5). These results verify that the proposed sequential SOI process can greatly improve the efficiencies of the SHW states which are very weak in the single crystal scheme[45]. By flipping the SAM states of the FWs before BBO2, as we did in Fig. 3(j–m), the Direct generated (Fig. 4(i, k)) and SOI-induced (Fig. 4(j, l)) SHWs in BBO2 carry another four angular momentum states, namely $(1, 0)_{\rm SHG}$, $(-1, 2)_{\rm SHG}$, $(1, 2)_{\rm SHG}$ and $(-1, 4)_{\rm SHG}$, corresponding to $(\sigma, 2\ell)_{\rm SHG}$, $(-\sigma, 2\ell + 2\sigma)_{\rm SHG}$, $(\sigma, 2\ell + 2\sigma)_{\rm SHG}$, and $(-\sigma, 2\ell + 4\sigma)_{\rm SHG}$, respectively. These states are also experimentally observed with uniform intensity distribution. Similar phenomena can be found in Fig. 4(e–h) and Fig. 4(m–p) when the angular momentum state of the FW is switched to $(-1, 0)_{\rm FW}$.

Since the four kinds of angular momentum states of FWs prepared before BBO2 have covered all the situations in this sequential crystal system, the angular momentum states of the generated SHWs are limited to eight types. It can be regarded as a "foldable" process, which means that the type of the angular momentum states of SHWs as well as their energy equality will not be affected by the number of sequential crystals. However, the amplitude and phase of the generated SHWs in each crystal may change with the number of the sequential crystals, which will affect the total efficiency. This method can be extended to the field of high-order harmonic generations. According to the symmetry selection rules of harmonic generation in nonlinear optics[50], under the incidence of FW with angular momentum state of $(\sigma, \ell)_{\rm FW}$, the allowed harmonic orders in the *c*-cut BBO crystal are $n = 3p\pm1$. The angular momentum states of $n^{\rm th}$-order harmonic waves are $(+\sigma, n\ell)_{\rm HHG}$ and $(-\sigma, n\ell)_{\rm HHG}$, corresponding to the cases where the circular polarization state of the harmonic wave is the same as or opposite to that of the FW. In the sequential process, the prepared angular momentum states of the FWs through the SOI process in BBO1 are $(\sigma, \ell)_{\rm FW}$ and $(-\sigma, \ell + 2\sigma)_{\rm FW}$. In the case where the circular polarization state of the harmonic wave is the same as that of the FW, the generated angular momentum states of $n^{\rm th}$-order harmonic waves in BBO2 are $(+\sigma, n\ell)_{\rm HHG}$ and $(-\sigma, n\ell + 2n\sigma)_{\rm HHG}$. Through the SOI process in BBO2, two new states of $n^{\rm th}$-order harmonic waves are generated, which are $(-\sigma, n\ell + 2\sigma)_{\rm HHG}$ and $(+\sigma, n\ell + 2n\sigma - 2\sigma)_{\rm HHG}$. Similarly, in the case where the circular polarization state of the harmonic wave is opposite to that of the FW, four kinds of the generated angular momentum states of $n^{\rm th}$-order harmonic waves in BBO2 are $(-\sigma, n\ell)_{\rm HHG}$, $(+\sigma, n\ell + 2n\sigma)_{\rm HHG}$, $(+\sigma, n\ell - 2\sigma)_{\rm HHG}$ and $(-\sigma, n\ell + 2n\sigma + 2\sigma)_{\rm HHG}$ in total. In addition, if the SAM flipping of the FW states prepared after BBO1 is considered, four new states of $n^{\rm th}$-order harmonic waves will be generated.

Conclusions

In summary, we propose a strategy to generate eight angular momentum states of SHWs through a sequential optical SOI in two uniaxial BBO crystals which have threefold rotational symmetry. With one input angular momentum state of the fundamental wave, one can prepare four kinds of FWs through linear optical SOI in the first BBO crystal and the manipulation of the SAM with a quarter-wave plate. Then, the FWs will be used to generate four angular momentum states of the SHWs in the second BBO crystal. As the SHWs also experience the linear optical SOI in the same crystal with a conversion efficiency close to 50%, we are able to generate eight angular momentum states of the SHWs with the double crystal system. These results are theoretically predicted and successfully verified in the experiment. The intensities of the eight SHW angular momentum states are uniformly distributed. It should be noted that the generated angular momentum states of SHWs by this approach are fixed. To realize flexible manipulation on the angular momentum states, it can be combined with conventional diffractive optical elements or spatial light modulators. The sequential optical SOI in the double crystal system can be also used to improve the energy distributions of

the photon-pairs with desired angular momentum states of light in the spontaneous down conversion[52], and similar concept can be extended to four-wave mixing and THz wave generation processes. This strategy is also applicative for other uniaxial nonlinear crystals. With the strong ability to prepare multiple angular momentum states, the proposed method may find more applications in optical communication, optical information processing and optical storage, etc.

Materials and methods

Nonlinear optical experiment

The sequential optical spin–orbit interaction process in the double BBO crystal system is investigated by using a home-made nonlinear optical system. The fundamental waves (FWs) with a wavelength 800 nm are from a femtosecond laser (repetition rate 80 MHz, pulse duration ~ 140 fs), whose polarization states are controlled by using a linear polarizer and a quarter-wave plate. After passing through an objective lens ($NA = 0.25$), the focused FWs are normally incident into the first BBO crystal (size: 6 mm × 6 mm, thickness 5 mm). The FWs and the generated second harmonic waves (SHWs) behind the first BBO crystal, which are collected by an objective lens ($NA = 0.25$) and circular polarization resolved by using a quarter-wave plate and a linear polarizer, are projected onto a camera by a tube lens (spherical or cylindrical lens). By removing the flip mirror (see Supplementary information Fig. S2), the polarization controlled FWs behind the first BBO crystal are subsequently focused into the second BBO crystal (size: 6 mm × 6 mm, thickness 5 mm) by an objective lens ($NA = 0.25$). The SHWs are collected by an objective lens ($NA = 0.25$) and resolved by using the polarization optics, which consist of a quarter-wave plate and a linear polarizer. Finally, the FWs and SHWs behind the second BBO crystal are projected by a tube lens (spherical or cylindrical lens) and captured by using a camera. To evaluate the energy distributions of different angular momentum states of linear and nonlinear optical waves, the quantitative characterization is also conducted. The power of the FWs is measured by using a power meter. The SHWs are captured by using an Andor spectrometer (SR193i), then by integrating the SHG spectra the relative power of the SHWs are obtained. It should be noted that the selection of objective lens with numerical aperture $NA = 0.25$ and thick β-BBO crystals is critical for the experiments, which has been investigated in ref.[45] and proved to be important for obtaining the angular momentum states of FWs with almost equal energy. In addition, the SAM states and the symmetry of intensity distribution of the generated SHWs are very sensitive to the angle between the incident light and the optical axis of the crystal, therefore, all the optical elements are finely adjusted to make the FWs normally incident into the BBO crystal.

References

1. Allen L, Beijersbergen MW, Spreeuw RJC et al. Orbital angular momentum of light and the transformation of Laguerre-Gaussian laser modes. *Phys Rev A* **45**, 8185–8189 (1992).
2. Hell SW, Wichmann J. Breaking the diffraction resolution limit by stimulated emission: stimulated emission-depletion fluorescence microscopy. *Opt Lett* **19**, 780–782 (1994).
3. Fürhapter S, Jesacher A, Bernet S et al. Spiral phase contrast imaging in microscopy. *Opt Express* **13**, 689–694 (2005).
4. He H, Friese MEJ, Heckenberg NR et al. Direct observation of transfer of angular momentum to absorptive particles from a laser beam with a phase singularity. *Phys Rev Lett* **75**, 826–829 (1995).
5. Paterson L, MacDonald MP, Arlt J et al. Controlled rotation of optically trapped microscopic particles. *Science* **292**, 912–914 (2001).
6. Grier DG. A revolution in optical manipulation. *Nature* **424**, 810–816 (2003).
7. Wang J, Yang JY, Fazal IM et al. Terabit free-space data transmission employing orbital angular momentum multiplexing. *Nat Photonics* **6**, 488–496 (2012).
8. Tan HY, Deng JH, Zhao RZ et al. A Free-space orbital angular momentum multiplexing communication system based on a metasurface. *Laser Photonics Rev* **13**, 1800278 (2019).
9. Ouyang X, Xu Y, Xian MC et al. Synthetic helical dichroism for six-dimensional optical orbital angular momentum multiplexing. *Nat Photonics* **15**, 901–907 (2021).
10. Mair A, Vaziri A, Weihs G et al. Entanglement of the orbital angular momentum states of photons. *Nature* **412**, 313–316 (2001).
11. Wang XL, Cai XD, Su ZE et al. Quantum teleportation of multiple degrees of freedom of a single photon. *Nature* **518**, 516–519 (2015).
12. Stav T, Faerman A, Maguid E et al. Quantum entanglement of the spin and orbital angular momentum of photons using metamaterials. *Science* **361**, 1101–1104 (2018).
13. Turnbull GA, Robertson DA, Smith GM et al. The generation of free-space Laguerre-Gaussian modes at millimetre-wave frequencies by use of a spiral phaseplate. *Opt Commun* **127**, 183–188 (1996).
14. Oemrawsingh SSR, van Houwelingen JAW, Eliel ER et al. Production and characterization of spiral phase plates for optical wavelengths. *Appl Opt* **43**, 688–694 (2004).
15. Marrucci L, Manzo C, Paparo D. Optical spin-to-orbital angular momentum conversion in inhomogeneous anisotropic media. *Phys Rev Lett* **96**, 163905 (2006).
16. Boruah BR. Dynamic manipulation of a laser beam using a liquid crystal spatial light modulator. *Am J Phys* **77**, 331–336 (2009).
17. Forbes A, Dudley A, McLaren M. Creation and detection of optical modes with spatial light modulators. *Adv Opt Photonics* **8**,

200–227 (2016).
18. Yu NF, Genevet P, Kats MA et al. Light propagation with phase discontinuities: generalized laws of reflection and refraction. *Science* **334**, 333–337 (2011).
19. Pu MB, Li X, Ma XL et al. Catenary optics for achromatic generation of perfect optical angular momentum. *Sci Adv* **1**, e1500396 (2015).
20. Xie X, Pu MB, Jin JJ et al. Generalized Pancharatnam-Berry phase in rotationally symmetric meta-atoms. *Phys Rev Lett* **126**, 183902 (2021).
21. Guo YH, Zhang SC, Pu MB et al. Spin-decoupled metasurface for simultaneous detection of spin and orbital angular momenta via momentum transformation. *Light Sci Appl* **10**, 63 (2021).
22. Wang B, Liu WZ, Zhao MX et al. Generating optical vortex beams by momentum-space polarization vortices centred at bound states in the continuum. *Nat Photonics* **14**, 623–628 (2020).
23. Gao XM, Yang LC, Lin H et al. Dirac-vortex topological cavities. *Nat Nanotechnol* **15**, 1012–1018 (2020).
24. Huang C, Zhang C, Xiao SM et al. Ultrafast control of vortex microlasers. *Science* **367**, 1018–1021 (2020).
25. Bliokh KY, Rodríguez-Fortuño FJ, Nori F et al. Spin–orbit interactions of light. *Nat Photonics* **9**, 796–808 (2015).
26. Cardano F, Marrucci L. Spin–orbit photonics. *Nat Photonics* **9**, 776–778 (2015).
27. Devlin RC, Ambrosio A, Rubin NA et al. Arbitrary spin-to-orbital angular momentum conversion of light. *Science* **358**, 896–901 (2017).
28. Ciattoni A, Cincotti G, Palma C. Circularly polarized beams and vortex generation in uniaxial media. *J Opt Soc Am A* **20**, 163–171 (2003).
29. Brasselet E, Izdebskaya Y, Shvedov V et al. Dynamics of optical spin-orbit coupling in uniaxial crystals. *Opt Lett* **34**, 1021–1023 (2009).
30. Forbes A, de Oliveira M, Dennis MR. Structured light. *Nat Photonics* **15**, 253–262 (2021).
31. Buono WT, Forbes A. Nonlinear optics with structured light. *Opto-Electron Adv* **5**, 210174 (2022).
32. Gui G, Brooks NJ, Kapteyn HC et al. Second-harmonic generation and the conservation of spatiotemporal orbital angular momentum of light. *Nat Photonics* **15**, 608–613 (2021).
33. Zdagkas A, McDonnell C, Deng JH et al. Observation of toroidal pulses of light. *Nat Photonics* **16**, 523–528 (2022).
34. Dholakia K, Simpson NB, Padgett MJ et al. Second-harmonic generation and the orbital angular momentum of light. *Phys Rev A* **54**, R3742–R3745 (1996).
35. Li GX, Wu L, Li KF et al. Nonlinear metasurface for simultaneous control of spin and orbital angular momentum in second harmonic generation. *Nano Lett* **17**, 7974–7979 (2017).
36. Wang L, Kruk S, Koshelev K et al. Nonlinear wavefront control with all-dielectric metasurfaces. *Nano Lett* **18**, 3978–3984 (2018).
37. Chen SM, Li KF, Deng JH et al. High-order nonlinear spin–orbit interaction on plasmonic metasurfaces. *Nano Lett* **20**, 8549–8555 (2020).
38. Liu S, Switkowski K, Xu CL et al. Nonlinear wavefront shaping with optically induced three-dimensional nonlinear photonic crystals. *Nat Commun* **10**, 3208 (2019).
39. Wei DZ, Wang CW, Xu XY et al. Efficient nonlinear beam shaping in three-dimensional lithium niobate nonlinear photonic crystals. *Nat Commun* **10**, 4193 (2019).
40. Shen YJ, Wang XJ, Xie ZW et al. Optical vortices 30 years on: OAM manipulation from topological charge to multiple singularities. *Light Sci Appl* **8**, 90 (2019).
41. Erhard M, Krenn M, Zeilinger A. Advances in high-dimensional quantum entanglement. *Nat Rev Phys* **2**, 365–381 (2020).
42. He C, Shen YJ, Forbes A. Towards higher-dimensional structured light. *Light Sci Appl* **11**, 205 (2022).
43. Chong A, Wan CH, Chen J et al. Generation of spatiotemporal optical vortices with controllable transverse orbital angular momentum. *Nat Photonics* **14**, 350–354 (2020).
44. Wang K, Titchener JG, Kruk SS et al. Quantum metasurface for multiphoton interference and state reconstruction. *Science* **361**, 1104–1108 (2018).
45. Tang YT, Li KF, Zhang XC et al. Harmonic spin–orbit angular momentum cascade in nonlinear optical crystals. *Nat Photonics* **14**, 658–662 (2020).
46. Chen CT, Wu BC, Jiang AD et al. A new-type ultraviolet SHG crystal: β-BaB_2O_4. *Sci Sin Ser B* **28**, 235–243 (1985).
47. Bhagavantam S, Chandrasekhar P. Harmonic generation and selection rules in nonlinear optics. *Proc Indian Acad Sci Sect A* **76**, 13–20 (1972).
48. Chen SM, Li GX, Zeuner F et al. Symmetry-selective third-harmonic generation from plasmonic metacrystals. *Phys Rev Lett* **113**, 033901 (2014).
49. Konishi K, Higuchi T, Li J et al. Polarization-controlled circular second-harmonic generation from metal hole arrays with threefold rotational symmetry. *Phys Rev Lett* **112**, 135502 (2014).
50. Li GX, Chen SM, Pholchai N et al. Continuous control of the nonlinearity phase for harmonic generations. *Nat Mater* **14**, 607–612 (2015).
51. Denisenko V, Shvedov V, Desyatnikov AS et al. Determination of topological charges of polychromatic optical vortices. *Opt Express* **17**, 23374–23379 (2009).
52. Wu YK, Tang YT, Hu ZX et al. Optical spin–orbit interaction in spontaneous parametric downconversion. *Optica* **10**, 538–543 (2023).

Acknowledgements

This work was supported by National Natural Science Foundation of China Grants (91950114 & 12161141010); National Key Technologies R&D Program of China (2022YFA1404301); Guangdong Provincial Innovation and Entrepreneurship Project Grant (2017ZT07C071); Natural Science Foundation of Shenzhen Innovation Commission Grant (JCYJ20200109140808088).

Author contributions

G. X. Li conceived the idea and supervised the project. Y. T. Tang and Z. X. Hu developed the theory and performed the computations. G. X. Li designed the experiments. Y. T. Tang, Z. X. Hu, K. F. Li and G. X. Li carried out the linear and nonlinear optical experiments. Y. T. Tang, Z. X. Hu and G. X. Li prepared the manuscript.

Competing interests

The authors declare no competing financial interests.

Supplementary information

Supplementary information for this paper is available at https://doi.org/10.29026/oea.2024.240138